Meteoritics & Planetary Science 42, Nr 12, 2055–2066 (2007)
Abstract available online at http://meteoritics.org

Reclassification and thermal history of Trenzano chondrite

A. M. FIORETTI[1*], M. C. DOMENEGHETTI[2], G. MOLIN[3], F. CÁMARA[4],
M. ALVARO[2], and L. AGOSTINI[5]

[1]CNR—IGG unità di Padova, corso Garibaldi 37, 35137 Padova, Italy
[2]Dipartimento di Scienze della Terra, Università di Pavia, via Ferrata 1, 27100 Pavia, Italy
[3]Dipartimento di Geoscienze, Università di Padova, via Giotto 1, 35137 Padova, Italy
[4]CNR—IGG unità di Pavia, via Ferrata 1, 27100 Pavia, Italy
[5]Liceo Scientifico Statale G. Galilei, viale San Giacomo 11, 37134 Verona, Italy
[*]Corresponding author. E-mail: anna.fioretti@igg.cnr.it

(Received 25 July 2006; revision accepted 25 May 2007)

Abstract–We present a new single-crystal X-ray diffraction (XRD) study performed on a suite of six orthopyroxene grains from the low-shocked H6 Trenzano meteorite. The quenched intracrystalline Fe^{2+}-Mg ordering state in orthopyroxene preserves the memory of the cooling rate near closure temperature T_c, thus yielding useful constraints on the last thermal event undergone by the host rock. The orthopyroxene T_c of 522 ± 13 °C, calculated using a new calibration equation obtained by Stimpfl (2005b), is higher than in previously published H chondrite data. The orthopyroxene cooling rate at this T_c is about 100 °C/kyr. This fast rate is inconsistent with the much slower cooling rate expected for H6 in the onion shell structural and thermal model of chondrite parent bodies. A petrographic study carried out at the same time indicated that the Trenzano meteorite is an H5 chondrite and not an H6 chondrite, as it is officially classified. Furthermore, the two-pyroxene equilibrium temperature of Trenzano (824 ± 24 °C), calculated with QUILF95, is similar to the two-pyroxene temperature of 750–840 °C obtained for the Carcote (H5) chondrite (Kleinschrot and Okrusch 1999).

INTRODUCTION

Understanding the relationship between the thermal histories of ordinary chondrites and petrologic types is critical in reconstructing the structural and thermal evolution of their parent body.

Structural and thermal models for chondrite parent bodies and their relationships with petrologic types have generated a great deal of discussion (Miyamoto et al. 1981; Scott and Rajan 1981; Grimm 1985; Taylor et al. 1987; Williams et al. 2000; Trieloff et al. 2003; Scott 2003; Rubin 2004; Grimm et al. 2005; Kessel et al. 2007). Two main structural models have been proposed for ordinary chondrite parent bodies. The onion-shell model relates the textural evolution of chondrites in the asteroid to increasing peak temperature and decreasing cooling rate proceeding from outer to inner, more insulated, shells (petrologic types from H3 to H6). However, metallographic cooling rates derived from Ni zoning in alloys (Taylor et al. 1987) and estimates of minimal cooling rates derived from intracrystalline Fe^{2+}-Mg exchange reaction in orthopyroxene (Folco et al. 1997) are inconsistent with this model.

The alternative rubble-pile model envisages that the final cooling of chondrites below the metallographic blocking temperature of ~500 °C took place in a structure generated after disruption and gravitational reassembling of the chondrite parent body, at an early stage of its metamorphic maturation (Scott and Rajan 1981).

The correlation between petrologic types and cooling rates at different temperatures observed for a group of exceptionally undisturbed (unshocked) ordinary H chondrites (Trieloff et al. 2003) suggested that reheating due to shock was the main cause of the lack of correlation found in previous works. Trieloff et al. (2003) obtained cooling rates of around 4.9 °C/Myr (H4), 3.6 °C/Myr (H5), and 3.3 °C/Myr (H6) in the 450–280 °C temperature range. Cooling rates at higher temperatures are less constrained but are on the order of 200 °C/Myr (H4), 30 °C/Myr (H5), and 10 °C/Myr (H6) in the temperature range between the respective peak metamorphic temperatures and ~450 °C, i.e., the closure temperature for Pb diffusion in phosphates.

Finally, further study of metallographic cooling rates in a large set of H chondrites (Scott 2003) and computer modelling of statistical distribution of chondrite peak temperatures and cooling rates for different fragmentation and reassembly conditions lead Grimm et al. (2005) to propose a third model, intermediate between onion-shell and rubble pile, which simultaneously accounts for both thermal structures. Kessel et al. (2007) observe that cooling rates at ~750 °C are much higher than cooling rates for temperatures ≤550 °C. They also point out that the restricted range of peak metamorphic temperatures revealed by olivine-spinel and two-pyroxene thermometry combined with the wide range of cooling rates at lower temperatures observed for H4 to H6 chondrites may indicate the existence of a major zone of transition of physical properties in the parent body, such as the base of a regolith pile. A final model maintains that no correlation exists between petrologic types and thermal history because chondrites represent distinct parent bodies (Yomogida and Matsui 1984; Ghosh et al. 2003).

Information on the cooling rate of chondrites can be derived from the intracrystalline Fe^{2+}-Mg exchange reaction between the octahedral sites in orthopyroxene; a reversible process that is orders of magnitude faster than intercrystalline Fe^{2+}-Mg diffusion. The quenched intracrystalline Fe^{2+}-Mg ordering state in orthopyroxene reflects the cooling rate near closure temperature T_c. Calibrations of $\ln k_D$ versus $1/T$ have been obtained experimentally in controlled fO_2 conditions for measuring the closure temperature of the Fe^{2+}-Mg exchange from the quenched ordering state of orthopyroxene samples with different compositions (Saxena and Ghose 1971; Molin et al. 1991; Yang and Ghose 1994; Stimpfl et al. 1999; Schlenz et al. 2001; Stimpfl 2005b).

Orthopyroxene cooling rates at the closure temperature T_c can be calculated on the basis of the kinetic approach proposed by Mueller (1967, 1969), who described the intracrystalline Fe^{2+}-Mg ordering reaction in this mineral as a homogeneous chemical reaction characterized by second-order kinetics. This method, developed by Ganguly (1982), involves the assumption of a continuous cooling model and calculation of time-constant values to produce the evolution of ordering state in the orthopyroxene from an initial T in a series of isothermal steps. The calculation requires both the use of a calibration $\ln k_D$ versus $1/T$ and of an Arrhenian expression for deriving the disordering rate constants as a function of T and X_{Fe}.

Studies of the degree of Fe^{2+}-Mg order in orthopyroxenes from terrestrial rocks and meteorites (Ganguly 1982; Ganguly et al. 1994; Molin et al. 1994; Ganguly and Domeneghetti 1996; Folco et al. 1996; 1997; Kroll et al. 1997; Zema et al. 1997; Domeneghetti et al. 2000; Ganguly and Stimpfl 2000; Stimpfl et al. 2005; McCallum et al. 2006; Domeneghetti et al. 2007) have proven effective in retrieving the thermal history of their host rocks. Applications of orthopyroxene single crystal X-ray diffraction (XRD) studies to chondrites (Molin et al. 1994; Folco et al. 1996, 1997) have shown a restricted orthopyroxene T_c range for each chemical group (e.g., 384 ± 48 to 480 ± 28 °C for H chondrites; 346 ± 27 to 459 ± 26 °C for L chondrites; and 340 ± 28 to 463 ± 17 °C for LL chondrites) and no systematic correlation with petrologic type. Cooling rate estimates around the T_c (103–105 °C/Myr), misquoted in Kessel et al. (2007), are two to three orders of magnitude faster than those obtained from metallographic and ^{244}Pu fission track data (Folco et al. 1997). Such fast cooling is in evident contrast with the observation that at temperatures below 500 °C, ordinary chondrite cooling rates are usually only a few °C/Myr (Kessel et al. 2007).

In this study, we calculate the closure temperature and the cooling rate of the ordinary chondrite Trenzano using the new equations experimentally obtained for orthopyroxene by Stimpfl (2005b) and Stimpfl et al. (2005). We present the new results, retrieved by six single-crystal XRD from six orthopyroxenes, and we compare them to previous data on ordinary H chondrites (Molin et al. 1994; Folco et al. 1996; 1997) recalculated using the same equations. The aim of our paper is to contribute to the understanding of thermal evolution of the ordinary chondrite parent body by clarifying thermal constraints.

Since the correct attribution of a chondrite to a specific petrologic type is essential when searching for possible correlations between metamorphic degree and thermal history, we also present the results of a petrographic study on five new thin sections of the Trenzano meteorite, officially classified as an H6 chondrite (Graham et al. 1985).

EXPERIMENTAL

Samples

Five new polished thin sections (pts) of the Trenzano chondrite were studied under transmitted and reflected light and checked against one standard, covered section from the Museum of Natural History, Vienna (Austria). Four of the new pts (T, T1, T2, and T3) were prepared from two distinct fragments stored in the Museum of Natural History of Brescia (Italy), and one section (T_TO) was kindly loaned by Prof. Roberto Compagnoni, Department of Earth Sciences, University of Turin (Italy). Orthopyroxene single crystals were selected from a small fragment (3.12 g) of the Trenzano meteorite from the Brescia Museum specimen. The chip was ground and sieved to yield a crystal separate with a grain size of about 150 μm. Extensive optical selection under the polarizing microscope revealed a few homogeneous, inclusion-free orthopyroxene crystals. Six of these, showing sharp diffraction profiles under the conventional X-ray diffractometer, were found to be suitable for XRD study.

Single-Crystal X-Ray Diffraction and Structure Refinement

Intensity data were collected on a three-circle Bruker AXS SMART APEX diffractometer, equipped with a CCD detector (graphite-monochromatized Mo*K*α radiation, λ = 0.71073 Å, 50 kV, 30 mA), with the Bruker SMART

Table 1. Cell parameters and information on data collection.

	a (Å)	*b* (Å)	*c* (Å)	*V* (Å3)	I_{tot}	I_{ind}	R_{int} (%)	Dimension (mm)
Opx Trenzano n.12	18.2571(5)	8.8507(2)	5.1955(1)	839.53(5)	9126	1226	1.9	0.050 × 0.090 × 0.160
Opx Trenzano n.13	18.2697(6)	8.8525(3)	5.1989(2)	840.83(5)	9127	1233	2.3	0.060 × 0.115 × 0.125
Opx Trenzano n.15	18.2690(10)	8.8542(5)	5.1985(3)	840.90(14)	9129	1233	1.8	0.075 × 0.115 × 0.180
Opx Trenzano n.16	18.2627(14)	8.8515(7)	5.1988(4)	840.39(19)	9139	1226	2.3	0.065 × 0.075 × 0.110
Opx Trenzano n.17	18.2658(15)	8.8554(8)	5.1973(4)	840.67(21)	9220	1228	2.3	0.135 × 0.110 × 0.075
Opx Trenzano n.18	18.2681(10)	8.8534(5)	5.1990(3)	840.87(13)	9129	1229	1.8	0.100 × 0.105 × 0.192

Note: standard deviations in brackets.

$R_{int} = \sum\left|F_o^2 - F_o^2(\text{mean})\right| / \sum(F_o^2)$; I_{ind} is the number of independent reflections used for structure refinements.

program. A total of 3600 frames (resolution 512 × 512 pixels) were collected with six different goniometer settings in the ω-scan mode (scan width = 0.3° ω; exposure time = 15 s frame^{-1}; detector-sample distance = 6.02 cm). Completeness of measured data was achieved up to 30° θ. The Bruker SAINT+ program was used for data reduction, including intensity integration as well as background and Lorentz-polarization corrections. The semi-empirical absorption correction of Blessing (1995), based on determination of transmission factors for equivalent reflections, was applied using the SADABS program (Sheldrick 1996) and the Laue group 2/*m*. Unit-cell parameters, obtained by a least-squares procedure that refines the position of about 900 reflections in the range of 12–22° θ are listed in Table 1. Reported in the same table is the value of discrepancy factor R_{int} calculated on the average of $(F_o)^2$ values of equivalent pairs in mmm Laue symmetry. For crystal n.13, which was found to contain an olivine inclusion, both orientation matrices of orthopyroxene and olivine were calculated, and the intensity data (about 22,000 reflections) of both phases were collected and integrated. After integration, orthopyroxene reflections which overlapped with olivine reflections were excluded from the $(F_o)^2$ list.

Some very weak (0*kl*) forbidden reflections were noted, with $k = 2n + 1$ and $l = 4n + 2$, which is consistent with *C*2/*c* clinopyroxene reflections exsolved on (100) and superimposed on the (0*kl*) forbidden orthopyroxene reflections. Structure refinement was carried out following Domeneghetti et al. (1996) for a *Pbca* phase co-existing with a *C*2/*c* exsolved phase but, due to the weakness of the forbidden reflections, it was not possible to calculate the fraction of *C*2/*c* phase in all crystals. The observed structure factor F_o^2 values were then treated by full-matrix least-squares refinement in the *Pbca* space group by SHELX-97 (Sheldrick 1998), with the individual weights and weighting scheme suggested by the program. Atomic scattering curves were taken from *International Tables for X-ray Crystallography* (Ibers and Hamilton 1974). Neutral versus ionized scattering factors were refined in all sites not involved in chemical substitutions (Hawthorne et al. 1995) and complete ionization for Mg and Fe in M1 and M2 sites. The extinction correction was applied using SHELX-97 (Sheldrick 1998). Table 1 also reports the number of total and independent reflections.

Electron Microprobe Analyses

Chemical composition of the single crystals used for XRD analysis, embedded in epoxy resin and polished, and of minerals in the pts were obtained using the Cameca Camebax Microbeam 799 and Cameca SX50 electron microprobes at CNR-IGG Padova. In both cases, operating conditions were 15 kV accelerating voltage and 15 nA beam current; counting times were 20 s at the peak and 10 s at the background. Spot size was 1 μm for all minerals except feldspar, for which a spot size of 3 μm was used to prevent diffusion loss of Na. The synthetic end-member mineral standards were: diopside for Mg, ferrosilite for Fe, wollastonite for Si and Ca, chromite for Cr, corundum for Al, and $MnTiO_3$ for Mn and Ti. A natural albite (Amelia albite) was used for Na. X-ray counts were converted into oxide weight percentages using the PAP (Pouchou and Pichoir 1991) correction program. Analyses are precise to within 1% for major elements and 3–5% for minor elements. For pyroxene, only those spot analyses with oxide totals of 100 ± 1.5, total cation contents of 4.000 ± 0.005 atoms on the basis of six oxygen atoms, and charge balance $3^{[4]}\text{Al} + \text{Na} - 3^{[6]}\text{Al} - 4\text{Ti} - 3\text{Cr} \leq |0.005|$ were selected and averaged. Silicate phase compositions determined on the pts are shown in Tables 2–5.

The chemical analyses of crystals n.12, n.13, and n.18 are listed in Table 6. Crystals n.15, n.16, and n.17 could not be analyzed because they were lost during polishing. For olivine, only those spot analyses with oxide totals of 100 ± 1.5 and total cation contents of 3.000 ± 0.005 atoms on the basis of four oxygen atoms were selected and averaged. Total cation contents of measured plagioclase, calculated on the basis of eight oxygen atoms, range from 4.97 to 5.01. Due to apparent compositional heterogeneity, their compositions were not averaged.

RESULTS

Petrography and Mineral Chemistry

The five polished thin sections show similar petrographic characters, indicating that the Trenzano meteorite is homogeneous. For this reason it is appropriate to describe the five pts together. The matrix is generally well recrystallized and the chondrules are mostly poorly defined, although

Table 2. Mean orthopyroxene composition of four Trenzano samples. Formulae are in atoms per formula unit (apfu) based on six oxygen atoms. Number of analyses per sample in parentheses.

Sample	T		T1		T3		T_TO	
No. of spots	(20)	St. dev.	(19)	St. dev.	(12)	St. dev.	(10)	St. dev.
SiO_2	56.56	0.51	56.57	0.37	56.76	0.37	57.39	0.36
TiO_2	n.d.		n.d.		n.d.		0.14	0.04
Al_2O_3	0.24	0.22	0.12	0.06	0.18	0.12	0.12	0.06
Cr_2O_3	0.14	0.11	0.10	0.05	0.15	0.16	0.08	0.02
FeO	11.26	0.30	11.02	0.22	11.12	0.16	10.94	0.22
MnO	0.53	0.09	0.46	0.06	0.50	0.07	0.48	0.03
MgO	31.16	0.31	31.33	0.19	31.38	0.20	31.69	0.18
CaO	0.64	0.13	0.61	0.10	0.60	0.14	0.60	0.09
Na_2O	0.03	0.06	0.01	0.02	0.01	0.02	0.01	0.01
Total	100.55		100.23		100.70		101.47	
Si	1.984		1.991		1.986		1.993	
Ti	n.d.		n.d.		n.d.		0.004	
Al	0.010		0.005		0.007		0.005	
Cr	0.004		0.003		0.004		0.002	
Fe	0.330		0.323		0.336		0.318	
Mn	0.016		0.014		0.015		0.014	
Mg	1.630		1.644		1.636		1.641	
Ca	0.024		0.023		0.022		0.022	
Na	0.002		0.002		0.001		0.001	
Total	4.000		4.004		4.007		4.000	
Woll %	1.21		1.16		1.13		1.12	
En %	82.05		82.76		82.21		82.24	
Fs %	16.63		16.08		16.66		16.64	

Table 3. Mean olivine composition of four Trenzano samples. Formulae are in atoms per formula unit (apfu) based on four oxygen atoms. Number of analyses per sample in parentheses.

Sample	T		T1		T3		T_TO	
No. of spots	(24)	St. dev.	(19)	St. dev.	(12)	St. dev.	(29)	St. dev.
SiO_2	39.40	0.31	39.28	0.22	39.32	0.17	39.97	0.28
Cr_2O_3	0.06	0.14	0.02	0.02	0.03	0.03	0.04	0.10
FeO	17.61	0.47	17.36	0.47	17.69	0.23	17.47	0.27
MnO	0.48	0.05	0.46	0.06	0.45	0.05	0.44	0.04
MgO	43.07	0.39	42.87	0.38	43.11	0.25	43.45	0.23
CaO	0.03	0.04	0.02	0.02	0.02	0.02	0.02	0.02
Total	100.66		100.03		100.62		101.43	
Si	0.996		0.998		0.995		1.000	
Cr	0.001		0.000		0.001		0.001	
Fe	0.372		0.369		0.374		0.366	
Mn	0.010		0.010		0.010		0.009	
Mg	1.623		1.624		1.626		1.621	
Ca	0.000		0.001		0.001		0.001	
Total	3.003		3.002		3.005		2.999	
Fo %	81.34		81.49		81.29		81.60	
Fa %	18.66		18.51		18.71		18.40	

readily delineated ones are also present (Fig. 1). Small fragmental chondrules and irregular clasts were also observed, suggesting that the Trenzano meteorite is brecciated on a subcentimetric scale. Turbid glass was identified in some of the chondrules, and monoclinic low-Ca pyroxene was detected in all pts, albeit in low quantities, indicating that inversion from monoclinic to orthorhombic enstatite was not completely achieved. Plagioclase is generally not well developed, and only in rare cases does it form discrete interstitial patches. Opaque phases are troilite, kamacite, and taenite. Metal represents about 10% and troilite up to 5% of the surface area of the pts. Small chromite grains were observed in all pts.

Orthopyroxene ($En_{82}Fs_{17}Wo_1$) and olivine (Fo_{81}) composition is identical, within error, in all the analyzed sections (Tables 2 and 3). Clinopyroxene is not frequent,

Table 4. Clinopyroxene composition of Trenzano samples T, T1, and T2. Formulae are in atoms per formula unit (apfu) based on six oxygen atoms.

Sample	T	T	T1	T1	T1	Avg.	St. dev.
Spot	C3	C5	C7	C8	C9		
SiO_2	54.38	55.08	54.25	55.04	54.65	54.68	0.38
TiO_2	n.d.	n.d.	n.d.	n.d.	n.d.		
Al_2O_3	0.45	1.15	0.51	0.52	0.85	0.70	0.3
Cr_2O_3	0.80	0.74	0.61	0.77	0.66	0.72	0.08
FeO	3.69	3.55	3.07	3.38	3.56	3.45	0.24
MnO	0.31	0.21	0.27	0.28	0.27	0.27	0.04
MgO	17.50	16.71	16.98	16.90	17.18	17.05	0.3
CaO	22.64	23.04	23.85	23.23	22.78	23.11	0.47
Na_2O	0.50	0.86	0.53	0.53	0.63	0.61	0.15
Total	100.27	101.35	100.06	100.64	100.59	100.59	0.49
Si	1.976	1.977	1.974	1.994	1.976	1.979	
Ti	n.d.	n.d.	n.d.	n.d.	n.d.		
Al	0.019	0.049	0.022	0.022	0.036	0.030	
Cr	0.023	0.021	0.018	0.022	0.019	0.021	
Fe	0.112	0.101	0.094	0.102	0.107	0.103	
Mn	0.010	0.007	0.008	0.008	0.008	0.008	
Mg	0.948	0.894	0.921	0.912	0.926	0.920	
Ca	0.881	0.886	0.930	0.902	0.882	0.896	
Na	0.035	0.060	0.037	0.037	0.044	0.043	
Total	4.005	4.000	4.004	4.000	4.000	4.002	
Woll %	45.17	46.79	47.63	46.83	45.86	46.46	
En %	48.58	47.23	47.16	47.40	48.13	47.70	
Fs %	6.25	5.96	5.20	5.75	6.01	5.83	

Table 5. Mean feldspar composition of three Trenzano samples. Formulae are in atoms per formula unit (apfu) based on eight oxygen atoms.

Sample	T	T	T_1	T_1	T_TO	T_TO
Spot	pl1	pl2	pl1	pl2	pl1	pl2
SiO_2	65.67	65.37	65.31	65.06	66.58	64.89
Al_2O_3	21.55	22.02	21.78	21.43	20.78	20.64
Cr_2O_3	0.02	0.02	0.02	0.02	0.01	0.02
FeO	0.46	0.50	0.15	0.21	0.38	0.44
CaO	2.68	3.13	2.54	2.46	1.79	3.17
Na_2O	8.77	8.30	9.85	9.27	9.35	9.19
K_2O	1.57	1.15	0.87	1.28	2.08	1.17
Total	100.79	100.88	100.52	99.73	100.97	99.51
Si	2.882	2.861	2.869	2.881	2.916	2.872
Al	1.115	1.136	1.128	1.119	1.072	1.077
Cr	0.001	0.001	0.001	0.001	0.000	0.001
Fe^{2+}	0.017	0.018	0.006	0.008	0.014	0.016
Ca	0.126	0.147	0.120	0.117	0.084	0.150
Na	0.746	0.704	0.839	0.796	0.794	0.788
K	0.088	0.064	0.049	0.072	0.116	0.066
Total	4.978	4.955	5.011	4.993	4.996	4.969
An %	13.12	16.04	11.87	11.85	8.44	14.95
Ab %	77.72	76.95	83.29	80.81	79.88	78.49
Or %	9.15	7.02	4.84	7.34	11.67	6.56

although small individuals were observed and analyzed in sections T, T1, and T2 (Table 4). Plagioclase composition is variable and not always strictly stoichiometric (Table 5). Cl apatite was identified by EDS analysis.

The co-existence of ortho- and clinopyroxenes (Tables 2 and 4) allowed equilibrium-temperature calculation for these two phases. Using QUILF95 (Andersen et al. 1993, modified for Windows in 1995), we obtained an equilibrium temperature of 824 ± 24 °C with an assumed pressure of 1 bar. This temperature is lower (although still within error) than the lowest value (865 ± 57 °C) of the equilibrium temperature range (865–926 °C; st. dev. 26.8) obtained, with the same

Table 6. Electron microprobe analyses and formulae in atoms per formula unit (apfu) based on six oxygen atoms.

	Opx	Opx	Opx
	n.12	n.13	n.18
Spots	14	5	10
SiO_2	57.31(22)	57.25(30)	57.03(15)
TiO_2	0.16(2)	0.17(4)	0.19(3)
Al_2O_3	0.23(4)	0.27(9)	0.30(4)
Cr_2O_3	0.16(5)	0.20(4)	0.22(5)
FeO	11.03(17)	11.08(13)	10.97(15)
MnO	0.50(7)	0.51(4)	0.48(4)
MgO	31.48(11)	31.52(32)	31.28(16)
CaO	0.61(5)	0.66(3)	0.61(5)
Na_2O	0.02(2)	0.02(2)	0.01(1)
Total	101.50	101.68	101.09
Si	1.991(4)	1.987(2)	1.989(4)
Ti	0.004(1)	0.005(1)	0.005(1)
Al	0.010(2)	0.011(4)	0.012(2)
Cr	0.005(1)	0.005(1)	0.006(1)
Fe^{2+}	0.320(5)	0.322(5)	0.320(4)
Mn	0.015(2)	0.015(1)	0.014(1)
Mg	1.630(6)	1.631(13)	1.627(7)
Ca	0.023(2)	0.024(1)	0.023(2)
Na	0.001(1)	0.001(1)	0.001(1)
Total	3.999	4.001	3.997
s.s.[a]	28.93	29.04	28.93
En %	82.56	82.44	82.56
Fs %	16.23	16.26	16.24
Wo %	1.15	1.24	1.16

[a] s.s. = calculated total site scattering in the M1 and M2 sites.

method and same pressure assumption (Slater-Reynolds and McSween 2005), on a series of petrologic type 6 H, L, and LL ordinary chondrites, and is within the two-pyroxene temperature (750–840 °C) obtained for Carcote H5 chondrite by Kleinschrot and Okrusch (1999).

Experimental data (Ashworth et al. 1984) show that above about 800 °C, the monoclinic polymorph of low-Ca pyroxene disappears if enough time is allowed for the transformation to the orthorombic phase. The Trenzano sample, however, shows minor relic striations of monoclinic low-Ca pyroxene consistent with lower peak metamorphic temperature.

Plagioclase composition (Table 5) from various grains is not uniform within the same pts ($Ab_{83–77}An_{9–16}Or_{5–12}$), suggesting this phase did not attain chemical equilibrium at the sample scale. The wide compositional range displayed by the Trenzano plagioclase is in better agreement with a petrologic type 5, although plagioclase heterogeneity has also been detected in type 6 chondrites (Nakamuta and Motomura 1999).

Shock-stage indicators (Stöffler et al. 1991) were checked in all pts. Most mineral grains show sharp optical extinction and irregular fractures. Grains with weak undulatory extinction are rare. Planar fractures are observed in only a few cases, and they never appear in sets of either parallel or intersecting lines. Plagioclase shows sharp optical extinction. Although Trenzano is described as a veined chondrite, we did not observe veins or melt pockets in any of the inspected thin sections. Our observations suggest that Trenzano should be classified as a very weakly shocked S2 chondrite. Rubin (2004) describes additional petrographic shock indicators in shock stage S2, type 5 and 6 ordinary chondrite. Of these, Trenzano only shows minor irregularly shaped troilite grains inside metal. Chromite is relatively frequent (up to 1% on modal visual estimation), but we did not observe it either in association with plagioclase or as veinlets traversing silicate grains—two features that appear to occur in all the H5, S2 chondrites analyzed by Rubin (2004).

Trenzano shows very minor alteration and may be assigned to the W0 class, following Wlotzka (1993).

Determination of Orthopyroxene Site Population, Closure Temperature, and Cooling Rate

Once structure refinement reached convergence, full-matrix least-squares cycles with chemical constraints, taken from the electron microprobe analysis and assuming 1σ as error, were carried out to obtain site partitioning. The site populations for crystals n.15 and n.16, which were lost during the chemical analysis procedure, were calculated using the chemical data from crystal n.12; this crystal showed very similar values for the mean atomic number (m.a.n.) at the M1 and M2 sites. The site population of crystal n.17 was calculated using the chemical analysis of crystal n.13. M1 and M2 site distribution was obtained by considering Mn totally ordered in the M2 site, taking into account the stronger preference for M2 of Mn compared to that of Fe^{2+} observed by Stimpfl (2005a) in a donpeacorite sample. The following restraints were also introduced into the refinement:

1. All structural sites were considered fully occupied;
2. Al was distributed between TB and M1 sites;
3. Cr^{3+} and Ti^{4+} were considered fully ordered at the M1 site;
4. Mg and Fe^{2+} were allowed to fractionate between the M1 and M2 sites;
5. Ca and Na were assumed to occupy the M2 site; and
6. The charge balance in isomorphous replacements was ensured by the equation:

$$X_{[6]_{Al}} + 2X_{Ti^{4+}} + X_{Cr} = X_{Na} + X_{[4]_{Al}} \qquad (1)$$

Discrepancy indices R_{all}, based on all the F_o^2, R_w, and goodness of fit (S), are listed in Table 7, which also gives the m.a.n. at the M1 and M2 sites obtained from the structure refinements before introducing chemical constraints, and observed mean bond distances for the M1 and M2 sites (<M1-O> and <M2-O>). It is evident from these structure parameters that the Trenzano orthopyroxenes are very homogeneous: the m.a.n. of the M1 and M2 sites and the

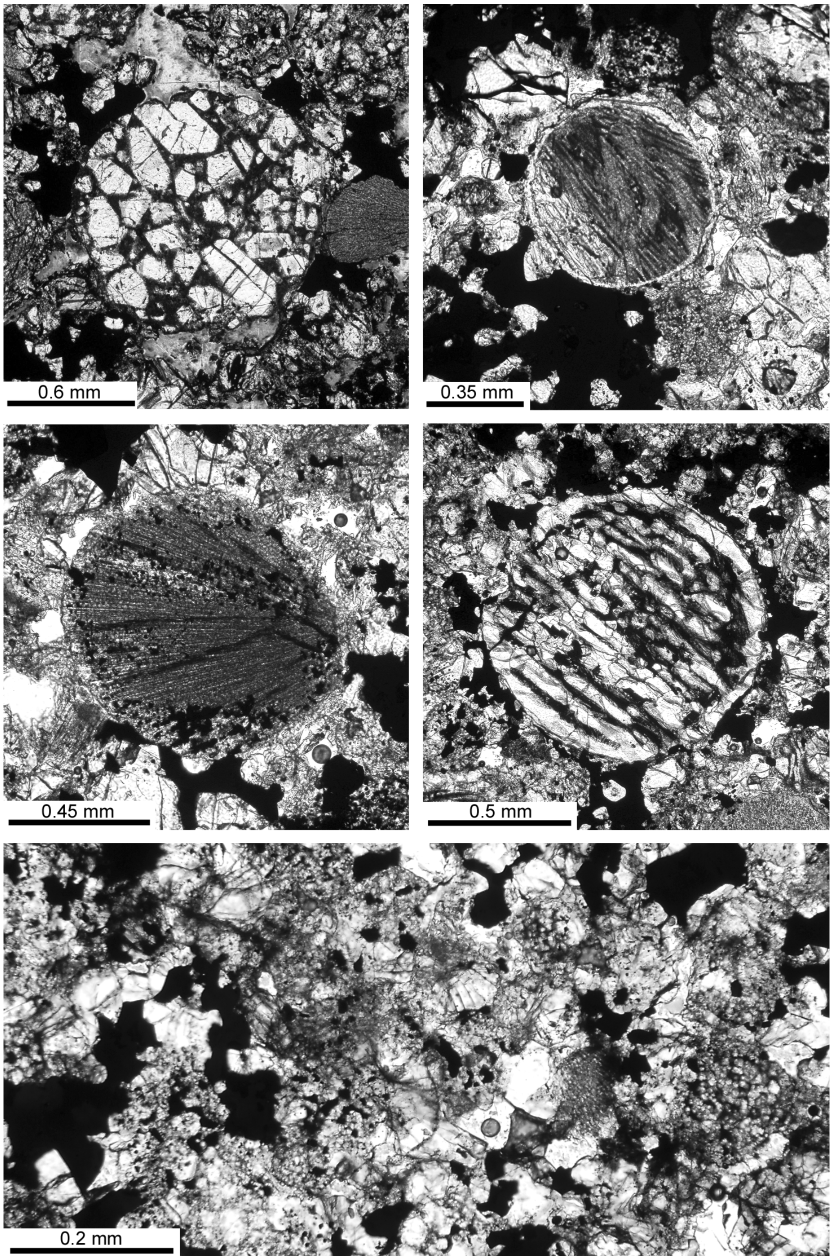

Fig. 1. Photomicrographs of Trenzano chondrite. The top and middle four micrographs show examples of readily delineated chondrules. The micrograph at the bottom illustrates the ghost of a poorly defined chondrule.

interatomic distances of all crystals are identical within estimated standard errors. Site populations are reported in Table 8; positional and atomic displacement parameters as well as observed and calculated structure factors are available from the authors.

For each crystal, the Fe^{2+}-Mg degree of order was estimated by means of the intracrystalline distribution coefficient k_D, expressed as:

$$k_D = X_{\mathrm{Fe}}^{\mathrm{M1}}(1-X_{\mathrm{Fe}}^{\mathrm{M2}})/X_{\mathrm{Fe}}^{\mathrm{M2}}(1-X_{\mathrm{Fe}}^{\mathrm{M1}}) \tag{2}$$

where $X_{\mathrm{Fe}}^{\mathrm{M1}} = (\mathrm{Fe})_{\mathrm{M1}}/(\mathrm{Fe} + \mathrm{Mg})_{\mathrm{M1}}$ and $X_{\mathrm{Fe}}^{\mathrm{M2}} = (\mathrm{Fe})_{\mathrm{M2}}/(\mathrm{Fe} + \mathrm{Mg})_{\mathrm{M2}}$. The k_D values of all crystals (Table 8) are very close, ranging from 0.043(4) to 0.052(3).

Closure temperature T_c of the Fe^{2+}-Mg exchange reaction was measured by the following equation:

$$\ln k_D = -2984(\pm 69)/T(K) + 0.747(\pm 0.078) \tag{3}$$

recently obtained by Stimpfl (2005b) by linear regression of $\ln k_D$(Fe-Mg) versus $1/T$ (K) data of low-Fe pyroxenes (Fs_{16}). For the Trenzano orthopyroxenes, T_c values (Table 8) range from 494(±18) to 532(±10) °C.

The calculation of the cooling rate for Trenzano crystals was carried out assuming that meteorites cooled according to

Table 7. Structural parameters.

	R_{all} (%)	R_w (%)	S	m.a.n. (M1)	m.a.n. (M2)	m.a.n. (M1 + M2)	<M1-O> (Å)	<M2-O> (Å)
Opx Trenzano n.12	2.10	4.92	1.125	12.36(3)	16.54(3)	28.90	2.081(1)	2.174(1)
Opx Trenzano n.13	2.46	5.72	1.177	12.45(3)	16.60(4)	29.05	2.081(1)	2.175(1)
Opx Trenzano n.15	2.45	5.58	1.184	12.40(3)	16.55(3)	28.95	2.082(1)	2.175(1)
Opx Trenzano n.16	2.28	4.97	1.140	12.39(3)	16.56(3)	28.95	2.081(1)	2.175(1)
Opx Trenzano n.17	2.85	6.36	1.134	12.44(4)	16.61(4)	29.05	2.082(1)	2.176(1)
Opx Trenzano n.18	1.96	4.72	1.149	12.36(3)	16.53(3)	28.89	2.082(1)	2.175(1)

Note: standard deviations in brackets.

$R_{\text{all}} = \sum\left|\left|F_o^2\right| - \left|F_c^2\right|\right| / \sum(F_o^2)$; $R_w = \{\sum[w(F_o^2 - F_c^2)^{1/2}] / \sum[w(F_o^2)^2]\}^{1/2}$; $S = \{\sum[w(F_o^2 - F_c^2)^2]/(n-p)\}^{0.5}$, where F_o and F_c are the observed and calculated structure factors, n is the number of reflections, and p is the total number of parameters refined; m.a.n. is the mean atomic number.

an asymptotic model: $1/T(\text{K}) = 1/T_o + \eta t$, where T_o is the initial temperature and η is the cooling time constant (Ganguly 1982). For this calculation, we used the above-reported Equation 3 obtained by Stimpfl (2005b) for low-iron samples (Fs_{16}) and Stimpfl et al.'s 2005 kinetic data. These authors obtained a new Arrhenian expression for the rate constant (C_oK^+) by means of kinetic experiments performed on orthopyroxene samples of different composition using WI buffer mixture, which takes into account the dependence of the rate constant on temperature and on X_{Fe} as follows:

$$\ln(C_oK^+) = (28.26 + 5.27\,X_{\text{Fe}}) - (41{,}511 - 12{,}600\,X_{\text{Fe}})/T(K),\ \text{min}^{-1} \tag{4}$$

The values of the cooling time constant are reported in Table 8. The resulting cooling rates $r = \eta \times (T_c)^2$, at the relevant closure temperatures T_c, range from 20 to 260 °C/kyr.

Table 9 reports the recalculated values of k_D, T_c, and the cooling rates of selected samples from the literature. The k_D values were obtained from the original site occupancy data by separating Mn from Fe^{2+} and by totally ordering Mn in M2, following Stimpfl (2005a) as for Trenzano orthopyroxene. With these new k_D values, the T_c and cooling rate were obtained using Equations 3 and 4.

DISCUSSION

Classification of the Trenzano Meteorite

The petrographic characters and the chemical composition of silicates in the Trenzano meteorite confirm that it belongs to the H ordinary chondrite group. However, they are not consistent with a petrologic type 6, in which primary turbid glass and monoclinic low-Ca pyroxene should not be present, chondrules should be extensively obliterated, and the rock should show good to excellent development of plagioclase (van Schmus and Wood 1967). Thus, the presence of turbid glass in some of the chondrules, the monoclinic status of some low-Ca pyroxene, and the scarce development of plagioclase indicate that Trenzano is not representative of the H6 petrologic type. For these reasons, we suggest that Trenzano should be reclassified and assigned to petrologic type H5. No significant petrographic differences were found in a comparison of our pts with a Trenzano pts kindly loaned by the Museum of Natural History, Vienna, which also seems to be a lower than petrologic type 6 (G. Kurat, personal communication).

Thermal History

The peak metamorphic temperature of Trenzano, as calculated with the QUILF95 geothermometer, is 824 ± 24 °C. This temperature is within the two-pyroxene temperature range (750–840 °C) obtained for the Carcote H5 chondrite (Kleinschrot and Okrusch 1999) and lower than the equilibrium temperature range (865–926 °C) reported for H6 chondrites (Slater-Reynolds and McSween 2005). Independent petrographic evidence indicates that Trenzano is an H5 ordinary chondrite. In the onion-shell model, the lower peak metamorphic temperature of Trenzano is consistent with a lower (H5) petrologic type.

Closure temperatures T_c of the Fe^{2+}-Mg exchange reaction in orthopyroxene obtained from six crystals (Table 8) range between 494 ± 18 and 532 ± 10 °C, and yield a weighted mean value of 522 ± 13° C. Corresponding cooling rates calculated from Trenzano individual orthopyroxene single crystals (Table 8) range between ~22 and ~260 °C/kyr, giving a mean value of 130 °C/kyr and a standard deviation of 80 °C/kyr. Because the six crystals we extracted from the small chip of Trenzano are chemically homogeneous and record the same thermal history, the large span observed is a consequence of the method of cooling rate calculation. Ganguly et al. (1989) remarked that for low-Fe orthopyroxene cooling rates, calculation is strongly sensitive to error in site occupancy data, even when the error is as low as ±0.002, as it is for Trenzano crystals. We must therefore conclude that, for this composition, the method can only provide an indication of the order of magnitude of the cooling rate.

The recalculated cooling rates of selected H4, H5, and H6 chondrites (Table 9) range from ~10 to ~165 °C/kyr and span the same orders of magnitude as those of the Trenzano individual single crystals. These data confirm that cooling

Table 8. Site populations, closure temperatures (T_c), cooling time constants (η), and cooling rates (r) at closure temperature.

	Opx Trenzano n.12	Opx Trenzano n.13	Opx Trenzano n.15	Opx Trenzano n.16	Opx Trenzano n.17	Opx Trenzano n.18
T site						
Si	1.991	1.988	1.990	1.990	1.987	1.988
Al	0.009	0.012	0.010	0.010	0.013	0.012
M1 site						
Mg	0.972(2)	0.967(2)	0.970(2)	0.971(2)	0.968(3)	0.972(2)
Fe	0.021(2)	0.023(2)	0.022(2)	0.022(2)	0.022(2)	0.019(2)
Al	0.000	0.000	0.000	0.000	0.000	0.000
Cr	0.003	0.006	0.004	0.004	0.005	0.005
Ti	0.004	0.004	0.004	0.004	0.005	0.004
M2 site						
Mg	0.660(2)	0.657(2)	0.660(2)	0.659(2)	0.656(2)	0.661(2)
Fe	0.300(3)	0.301(2)	0.300(3)	0.301(3)	0.303(3)	0.300(2)
Ca	0.023	0.025	0.023	0.023	0.024	0.023
Mn	0.015	0.015	0.015	0.015	0.015	0.014
Na	0.002	0.002	0.002	0.002	0.002	0.001
X_{Fe}^{M1}	0.0211	0.0232	0.0222	0.0222	0.0222	0.0192
X_{Fe}^{M2}	0.3125	0.3142	0.3125	0.3135	0.3160	0.3122
k_D	0.0475(45)	0.0519(25)	0.0499(50)	0.0496(47)	0.0492(51)	0.0431(38)
$\ln k_D$	−3.0464	−2.9581	−2.9978	−3.0037	−3.0118	−3.1449
T_c (°C)	514 ± 20	532 ± 10	524 ± 21	523 ± 20	521 ± 22	494 ± 18
η (K^{-1}yr^{-1}) × 10^{-6}	0.1278	0.3993	0.2384	0.2218	0.2076	0.0370
r_{bestfit} (°C/yr)	0.0791	0.2587	0.1514	0.1402	0.1309	0.0217
$r_{\max}$ (°C/yr)	0.3004	0.8938	0.5466	0.5071	0.4719	0.0928
$r_{\min}$ (°C/yr)	0.0185	0.0705	0.0377	0.0350	0.0326	0.0055

Note: standard deviations in brackets.

$X_{\mathrm{Fe}}^{\mathrm{M1}}$ = (Fe)$_{\mathrm{M1}}$/(Fe + Mg)$_{\mathrm{M1}}$; $X_{\mathrm{Fe}}^{\mathrm{M2}}$ = (Fe)$_{\mathrm{M2}}$/(Fe + Mg)$_{\mathrm{M2}}$; $k_D = X_{\mathrm{Fe}}^{\mathrm{M1}}(1 - X_{\mathrm{Fe}}^{\mathrm{M2}})/X_{\mathrm{Fe}}^{\mathrm{M2}}(1 - X_{\mathrm{Fe}}^{\mathrm{M1}})$.

Table 9. Values of k_D, closure temperature (T_c), and cooling rate (r_{bestfit}) of orthopyroxene from a set of H4, H5, and H6 chondrites. FM76(15) and FM76(18) are two crystals from the same H4 chondrite sample. T_c and cooling rates are recalculated from literature data.

	FM76[a] (15)	FM76[a] (18)	FM49[a] (9)	Zaoyang[b]	FM156[a] (2)
Type	H4	H4	H5	H5	H6
k_D	0.034	0.0494	0.0356	0.0504	0.0424
T_c (°C)	450	522	458	526	491
r_{bestfit} (°C/kyr)	10	130	170	165	210

[a]Data from Folco et al. 1996.
[b]Data from Molin et al. 1994.

rates of equilibrated H chondrites near their closure temperature T_c (450–550 °C) is in all cases very fast compared to Trieloff et al. (2003), and is independent of the petrologic type, as observed by Folco et al. (1997).

The observed cooling rate at around 520 °C of Trenzano could indicate fast cooling after shock-reheating, or cooling in a shallow environment, possibly caused by denudation as a consequence of excavation of formerly overlying rocks or by fragmentation of the parent body into sizable blocks. Estimation of the depth level corresponding to the cooling rate of ~130 °C/kyr can only be approximate, as this calculation depends on the choice of boundary conditions (Warren et al. 1991), which are at present unconstrained. We obtain a burial depth of ~50–100 m, tentatively assuming ~800° C as the initial temperature, 0 °C as the surface temperature of the parent asteroid, and 31.5 m^2/yr as the thermal diffusivity of the rock (Warren et al. 1991).

Trieloff et al. (2003) showed that the cooling rate for an unshocked H5 chondrite in the temperature range between its peak metamorphic temperature and ~450 °C, which is the closure temperature for Pb-Pb age in phosphates, is ~30 °C/Myr. The cooling rate retrieved from the Fe-Mg quenched ordering state in the orthopyroxene at T_c (~520 °C) is three orders of magnitude faster. Impact shock metamorphism may play an essential role in the thermal history of chondrites (Stöffler et al. 1991; Rubin 2004). Shock heating and annealing may obscure pre-shock thermal history and, depending on the highest temperature reached during shock, may selectively disorder specific mineral closing temperatures. However, Trenzano is an S2 chondrite, and such weakly shocked meteorites are not expected to have undergone significant reheating due to shock (Folco et al. 1997). According to Rubin (2004), all ordinary chondrites reached shock stage S3–S6 due to collisional events and then underwent post-shock annealing, which not only obliterated most of their primary shock features but also contributed significantly to the final thermometamorphism displayed. Rubin (2004) states that it is possible for an ordinary chondrite to be shocked and subsequently annealed to a stage at which it appears less shocked than it was at an earlier point in its history. This may result in incorrect definition of shock stage and consequent thermal implications.

If this were the case, it is essential to test the expected correlation between orthopyroxene cooling rate and petrologic type on a set of unquestionably unshocked ordinary chondrites, e.g., those used by Trieloff et al. (2003).

SUMMARY AND CONCLUSIONS

We examined the petrographic characters and mineral compositions of five new thin sections from the weakly shocked (S2) Trenzano chondrite and found characteristics indicating that an H5 classification would be more appropriate than the present H6 ordinary chondrite classification.

The QUILF95 geothermometer yielded an equilibrium temperature of 824 ± 24 °C, which is within the temperature range obtained for Carcote H5 chondrite (Kleinschrot and Okrusch 1999).

Based on the Fe^{2+}-Mg ordering state as measured by single-crystal XRD on six distinct crystals, we obtained an orthopyroxene closure temperature of 522 ± 13 °C, corresponding to a cooling rate of ~130 °C/kyr at fO_2 of WI. The calculated T_c and cooling rate are within the range of those reported in the literature for H4–H6 ordinary chondrites, and are apparently independent of their petrologic type.

This is inconsistent with the onion-shell asteroid model, and either points to now-obliterated shock-induced thermal effects (Rubin 2004) or indicates that the asteroid parent-body structure was more complicated than that posited by the onion-shell model (Williams et al. 2000; Grimm et al. 2005; Kessel et al. 2007).

Acknowledgments–This study was supported by the Italian Antarctic Research Program (PNRA), Pavia University "Fondo di Ateneo per la Ricerca" (F.A.R. grant 2004), and CNR project TA.PO1.004.002. We thank R. Gastoni and R. Carampin for their assistance during sample preparation and microprobe analyses, respectively. We thank R. Carampin for his assistance during microprobe analyses. We are grateful to reviewers M. Stimpfl and M. Tribaudino, to associate editor K. Righter, and to editor-in-chief A. J. T. Jull for their useful comments. We thank the "Museo di Scienze" of the city of Brescia for providing us a sample of Trenzano chondrite.

Editorial Handling—Dr. Kevin Righter

REFERENCES

Andersen D. J., Lindsley D. H., and Davidson P. M. 1993. QUILF: A Pascal program to assess equilibria among Fe-Mg-Mn-Ti oxides, pyroxenes, olivine, and quartz. *Computer and Geosciences* 19:1333–1350.

Ashworth J. R., Mallinson L. G., Hutchinson R., and Biggar G. M. 1984. Chondrite thermal histories constrained by experimental annealing of Quenggouk orthopyroxene. *Nature* 308:259–261.

Bischoff A. and Stöffler D. 1992. Shock metamorphism as a fundamental process in the evolution of planetary bodies: Information from meteorites. *European Journal of Mineralogy* 4: 707–755.

Blessing R. H. 1995. An empirical correction for absorption anisotropy. *Acta Crystallographica* A51:33–38.

Domeneghetti M. C., Tazzoli V., Boffa Ballaran T., and Molin G. M. 1996. Orthopyroxene from the Serra de Magé meteorite: A structure refinement procedure for a Pbca phase coexisting with a *C*2/*c* exsolved phase. *American Mineralogist* 81:842–846.

Domeneghetti M. C., Molin G. M., Triscari M., and Zema M. 2000. Orthopyroxene as a geospeedometer: Thermal history of Kapoeta, Old Homestead 001, and Hughes 002 howardites. *Meteoritics & Planetary Science* 35:347–354.

Domeneghetti M. C., Fioretti A. M., Cámara F., Molin G. M., and Tazzoli V. 2007. Thermal history of ALH 84001 meteorite by Fe^{2+}-Mg ordering in orthopyroxene. *Meteoritics & Planetary Science* 42:1703–1710.

Folco L., Mellini M., and Pillinger C. T. 1996. Unshocked equilibrated H chondrites: A common low-temperature record from orthopyroxene iron-magnesium ordering. *Meteoritics & Planetary Science* 31:388–393.

Folco L., Mellini M., and Pillinger C. T. 1997. Equilibrated ordinary chondrites: Constraints for thermal history from iron-magnesium ordering in orthopyroxene. *Meteoritics & Planetary Science* 32: 567–575.

Ganguly J. 1982. Fe^{2+}-Mg order-disorder in ferromagnesian silicates. In *Thermodynamics: Kinetics and geological applications*, edited by Saxena S. K. Advances in Physical Geochemistry, vol. 2. Berlin: Springer. pp. 58–99.

Ganguly J., Bose K., and Ghose S. 1989. Fe^{2+}-Mg ordering in orthopyroxene and the cooling rates of meteorites (abstract). 20th Lunar and Planetary Science Conference. pp. 331–332.

Ganguly J., Yang H., and Ghose S. 1994. Thermal history of mesosiderites: Quantitative constraints from compositional zoning and Fe-Mg ordering in orthopyroxenes. *Geochimica et Cosmochimica Acta* 58:2711–2723.

Ganguly J. and Domeneghetti M. C. 1996. Cation ordering of orthopyroxenes from the Skaergaard Intrusion: Implications for the subsolidus cooling rates and permeabilities. *Contributions to Mineralogy and Petrology* 122:359–367.

Ganguly J. and Stimpfl M. 2000. Cation ordering in orthopyroxenes from two stony iron meteorites: Implications for cooling rates and metal-silicate mixing. *Geochimica et Cosmochimica Acta* 64:1291–1292.

Ghosh A., Weidenschilling S. J., and McSween H. Y. Jr. 2003. Importance of accretion process in asteroid thermal evolution: H6 Hebe as an example. *Meteoritics & Planetary Science* 38: 711–724.

Grimm R. E. 1985. Penecontemporaneous metamorphism, fragmentation, and reassembly of ordinary chondrite parent bodies. *Journal of Geophysical Research* 90:2022–2028.

Grimm W. F., Bottke D., Enke B., Scott E. R. D., Asphaug E., and Richardson D. 2005. Joint thermal and collisional modeling of the H chondrite parent body (abstract #1798). 36th Lunar and Planetary Science Conference CD-ROM.

Graham A. L., Bevan A. W. R., and Hutchinson R. 1985. *Catalogue of meteorites: With special reference to those represented in the collection of the British Museum (Natural History).* Tucson, Arizona: The University of Arizona Press. 460 p.

Hawthorne F. C., Ungaretti L., and Oberti R. 1995. Site populations in minerals: Terminology and presentation of results of crystal-structure refinement. *Canadian Mineralogist* 33:907–911.

Ibers J. A. and Hamilton W. C., editors. 1974. *International tables for X-ray crystallography*, vol. 4. Birmingham, UK: Kynoch Press. pp. 99–101.

Kessel R., Beckett J. R., and Stolper E. M. 2007. The thermal history of equilibrated ordinary chondrites and the relationship between textural maturity and temperature. *Geochimica et Cosmochimica Acta* 71:1855–1881.

Kleinschrot D. and Okrusch M. 1999. Mineralogy, petrography, and thermometry of the H5 chondrite Carcote, Chile. *Meteoritics & Planetary Science* 34:795–802.

Kroll H., Lueder T., Schlenz H., Kirfel A., and Vad T. 1997. The Fe^{2+}, Mg distribution in orthopyroxene: A critical assessment of its potential as a geospeedometer. *European Journal of Mineralogy* 9:705–733.

McCallum I. S., Schwartz J. M., Domeneghetti M. C., Zema M., Cámara F., McCammon C., and Ganguly J. 2006. Cooling history of lunar Mg-suite gabbronorite 76255, troctolite 76535, and Stillwater pyroxenite SC-936: The record in exsolution and ordering in pyroxenes. *Geochimica et Cosmochimica Acta* 70: 6068–6078.

Miyamoto M., Fujii N., and Takeda H. 1981. Ordinary chondrite parent body: An internal heating model. Proceedings, 12th Lunar and Planetary Science Conference. pp. 1145–1152.

Molin G. M., Saxena S. K., and Brizi E. 1991. Iron-magnesium order-disorder in an orthopyroxene crystal from the Johnstown meteorite. *Earth and Planetary Science Letters* 105:260–265.

Molin G. M., Tribaudino M., and Brizi E. 1994. Zaoyang chondrite cooling history from Fe^{2+}-Mg intracrystalline ordering in pyroxenes. *Mineralogical Magazine* 58:143–150.

Mueller R. F. 1967. Model for order-disorder kinetics in certain quasi-binary crystals of continuously variable composition. *Journal of Physics and Chemistry of Solids* 28:2239–2243.

Mueller R. F. 1969. *Kinetics and thermodynamics of intracrystalline distribution*. Mineralogical Society of America Special Paper 2. pp. 83–93.

Nakamuta Y. and Motomura Y. 1999. Sodic plagioclase thermometry of type 6 ordinary chondrites: Implications for the thermal histories of parent bodies. *Meteoritics & Planetary Science* 34:763–772.

Pouchou J. L. and Pichoir F. 1991. Quantitative analysis of homogeneous or stratified microvolumes applying the model "PAP." In *Electron probe quantitation*, edited by Heinrich K. F. J. and Newbury D. E. New York: Plenum Press. pp. 31–75.

Rubin A. 2004. Postshock annealing and postannealing shock in equilibrated ordinary chondrites: Implications for the thermal and shock histories of chondritic asteroids. *Geochimica et Cosmochimica Acta* 68:673–689.

Saxena S. K. and Ghose S. 1971. Mg^{2+}-Fe^{2+} order-disorder and the thermodynamics of the orthopyroxene crystalline solution. *American Mineralogist* 56:532–559.

Schlenz H., Kroll H., and Phillips M. W. 2001. Isothermal annealing and continuous cooling experiments on synthetic orthopyroxenes: Temperature and time evolution of the Fe,Mg distribution. *European Journal of Mineralogy* 13:715–726.

Scott E. R. D. 2003. Metallographic cooling rates of H chondrites and the structure of their parent asteroid (abstract #5293). *Meteoritics & Planetary Science* 38:A151.

Scott E. R. D. and Rajan R. S. 1981. Metallic minerals, thermal histories, and parent bodies of some xenolithic, ordinary chondrite meteorites. *Geochimica et Cosmochimica Acta* 45:53–67.

Sheldrick G. M. 1996. SADABS. Institüt für Anorganische Chemie der Universität, Göttingen, Germany.

Sheldrick G. M. 1998. SHELX97—Programs for crystal structure analysis (Release 97-2). Institüt für Anorganische Chemie der Universität, Göttingen, Germany.

Slater-Reynolds V. and McSween H.Y. Jr. 2005. Peak metamorphic temperatures in type 6 ordinary chondrites: An evaluation of pyroxene and plagioclase geothermometry. *Meteoritics & Planetary Science* 40:745–754.

Stimpfl M., Ganguly J., and Molin G. M. 1999. Fe^{2+}-Mg order-disorder in orthopyroxene: Equilibrium fractionation between the octahedral sites and thermodynamic analysis. *Contributions to Mineralogy and Petrology* 136:297–309.

Stimpfl M. 2005a. The Mn, Mg-intracrystalline exchange reaction in donpeacorite ($Mn_{0.54}Ca_{0.03}Mg_{1.43}Si_2O_6$) and its relation to the fractionation behavior of Mn in Fe,Mg-orthopyroxene. *American Mineralogist* 90:155–161.

Stimpfl M. 2005b. Erratum: The Mn,Mg-intracrystalline exchange reaction in donpeacorite ($Mn_{0.54}Ca_{0.03}Mg_{1.43}Si_2O_6$) and its relation to the fractionation behavior of Mn in Fe,Mg-orthopyroxene. *American Mineralogist* 90:776.

Stimpfl M., Ganguly J., and Molin G. M. 2005. Fe^{2+}-Mg order-disorder in orthopyroxene: Experimental studies and applications to cooling rates of rocks. *Contributions to Mineralogy and Petrology* 150:319–334.

Stöffler D., Keil K., and Scott E. R. D. 1991. Shock metamorphism of ordinary chondrites. *Geochimica et Cosmochimica Acta* 55: 3845–3867.

Taylor G. J., Maggiore P., Scott E. R. D., Rubin A. E., and Keil K. 1987. Original structures, and fragmentation and reassembly histories of asteroids: Evidence from meteorites. *Icarus* 69:1–13.

Trieloff M., Jessberger E. K., Herrwerth I., Hopp J., Fiéni C., Ghélis M., Bourot-Denise M., and Pellas P. 2003. Structure and thermal history of H chondrite parent asteroid revealed by thermochronometry. *Nature* 422:502–506.

Van Schmus W. R. and Wood J. A. 1967. A chemical-petrologic classification for the chondritic meteorites. *Geochimica et Cosmochimica Acta* 31:747–765.

Warren P. H., Haack H., and Rasmussen K. L. 1991. Megaregolith insulation and the duration of cooling to isotopic closure within differentiated asteroids and the Moon. *Journal of Geophysical Research* 96:5909–5923.

Williams C. V., Keil K., Taylor G. J., and Scott E. R. D. 2000. Cooling rates of equilibrated clasts in ordinary chondrite regolith breccia: Implications for the parent body history. *Chemie der Erde* 59:287–305.

Wlotzka F. 1993. A weathering scale for the ordinary chondrites (abstract). *Meteoritics* 28:460.

Yang H. and Ghose S. 1994. In situ Fe-Mg order-disorder studies and thermodynamic properties of orthopyroxenes (Fe, Mg)$_2$Si$_2$O$_6$. *American Mineralogist* 79:633–643.

Yomogida K. and Matsui T. 1984. Multiple parent bodies of ordinary chondrites. *Earth and Planetary Science Letters* 68: 34–42.

Zema M., Domeneghetti M. C., Molin G. M., and Tazzoli V. 1997. Cooling rates of diogenites: A study of Fe^{2+}-Mg ordering in orthopyroxene by X-ray single-crystal diffraction. *Meteoritics & Planetary Science* 32:855–862.